Supplementary materials for Phononic Helical Nodal Lines with $\mathcal{PT}$ Protection in MoB_2

T. T. Zhang,[1,2,3,4] H. Miao,[5,*] Q. Wang,[6] J. Q. Lin,[5,2,7] Y. Cao,[8] G. Fabbris,[8] A. H. Said,[8] X. Liu,[7] H. C. Lei,[6,†] Z. Fang,[1,9] H. M. Weng,[1,9,‡] and M. P. M. Dean[5,§]

[1]*Institute of Physics, Chinese Academy of Sciences, Beijing 100190, China*
[2]*University of Chinese Academy of Sciences, Beijing 100049, China*
[3]*Department of Physics, Tokyo Institute of Technology, Ookayama, Meguro-ku, Tokyo 152-8551, Japan*
[4]*Tokodai Institute for Element Strategy, Tokyo Institute of Technology, Nagatsuta, Midori-ku, Yokohama, Kanagawa 226-8503, Japan*
[5]*Condensed Matter Physics and Materials Science Department, Brookhaven National Laboratory, Upton, New York 11973, USA*
[6]*Department of Physics and Beijing Key Laboratory of Opto-Electronic Functional Materials and Micro-devices, Renmin University of China, Beijing, China*
[7]*School of Physical Science and Technology, ShanghaiTech University, Shanghai 201210, China*
[8]*Advanced Photon Source, Argonne National Laboratory, Argonne, Illinois 60439, USA*
[9]*Collaborative Innovation Center of Quantum Matter, Beijing 100084, China*

CALCULATION DETAILS

Irreducible representations are calculated by the open source code in Ref. [1] with conventions following the BCS server [2]. After obtaining the second-rank tensor of force constants by the Vienna *ab initio* simulation package (VASP)[3], a standard Fourier transformation is applied to get the eigenvalues and eigenvectors, which are used to calculate the phonon dispersion. An energy difference of 10^{-4} meV is set to search for band crossings. Two endless nodal lines are found in the Brillouin zone. Berry phase and surface states are calculated by open source package WannierTools [4], which verifies the existence of $\mathcal{PT}$-protected nodal lines.

The dynamic structure factor, $S^{DFPT}(\mathbf{Q},\omega)$, of MoB_2 is calculated using Eq. 3 and 4 in the main text. The Debye-Waller factor is omitted from Eq. 4 of the main text as it plays a minor role in the relative mode intensity [5, 6]. It should be noted that the phonon DSF is a function of total momentum transfer, $\boldsymbol{Q}$, not the reduced momentum, $\boldsymbol{q} = \boldsymbol{Q} - \tau$, where τ is the reciprocal lattice vector. Therefore, the DSF is inequivalent in different Brillouin zones. A direct comparison of the phonon dispersion and $S^{DFPT}(\mathbf{Q},\omega)$ along the (7,7,7)→(8,8,8), (7,7,7)→(7,7.5, 6.5) and (7.5,7.5,7.5)→(7.5,8,7) directions is shown in Fig. S1.

The phonon surface states of MoB_2 are calculated by the Green's function method that is widely used in calculating the surface states of topological materials [4, 7, 8]. Here we provide more details about this method. We first perform first principles calculations to obtain the second-order rank tensor of force constants. Then, we construct a semi-infinite 3D slab model with an explicit surface, for example the [010] surface in our paper. The top-layer Green's function of the semi-infinite model can thus be derived from the force constants by iterative method. Finally, we take the imaginary part of the top-layer Green's function as the local density of states (LDOS). LDOS obtained by this method contains modes that are unique to the surface and modes that are related to bulk modes.

CRYSTAL STRUCTURE

Figure S2 shows x-ray diffraction (XRD) data of powder MoB_2 at room temperature. The structure refinement (red curve) gives a=b=3.013 Å, c=20.960 Å and is consistent with space group No. 166 [9, 10].

Space group No. 191 is observed for several transition metal diborides such as MgB_2 and ZrB_2. As a check we calculated the phonon spectra of MoB_2 with space group No. 191. Fig. S3 shows the calculated result, which contains negative modes corresponding an unstable ground state. Moreover, the phonon dispersion at positive energy is very different from our experimental data shown in the main text. We therefore conclude space group No.191 is not a stable ground state of MoB_2. Interestingly, our phonon spectra calculation of MgB_2 with space group No. 191 show topological nodal lines. However, in this case, the nodal lines are protected by crystal symmetries not the $\mathcal{PT}$ symmetry. In addition, the topological surface states of MgB_2 overlap with the bulk states [11] and may not be as robust as the surface states in MoB_2.

Finally, we note that beside inelastic x-ray scattering, the phonon spectrum near the zone center can be measured by Raman and infrared spectroscopy. The full phonon dispersion can, in principle, be measured by inelastic neutron scattering (INS). However, since boron in its natural abundance includes a large fraction of ^{10}B, which is known to be a strong neutron absorber, isotopically pure ^{11}B would be needed for INS measurements.

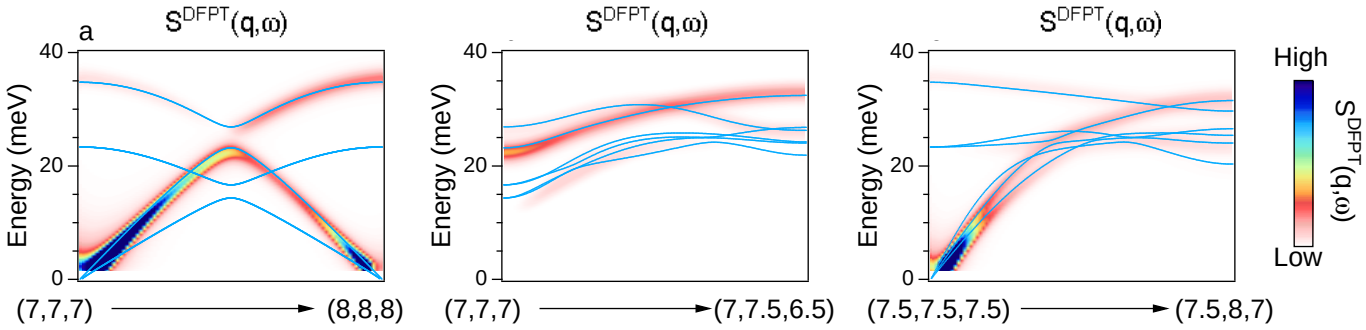

Figure S1. Experimental resolution-convoluted $S^{DFPT}(\mathbf{Q},\omega)$ along the (7,7,7)→(8,8,8), (7,7,7)→(7,7.5,6.5) and (7.5,7.5,7.5)→(7.5,8,7) directions are shown in (a)-(c). Blue curves are phonon dispersions.

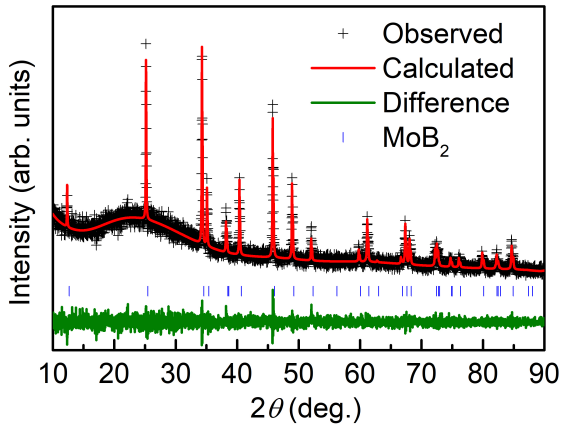

Figure S2. Powder XRD of MoB_2 measured with Cu K_α (λ=0.15406 nm) radiation. The red curve is the calculated XRD intensity. The cyan curve shows the difference between the raw data ("+" mark) and the calculated intensity.

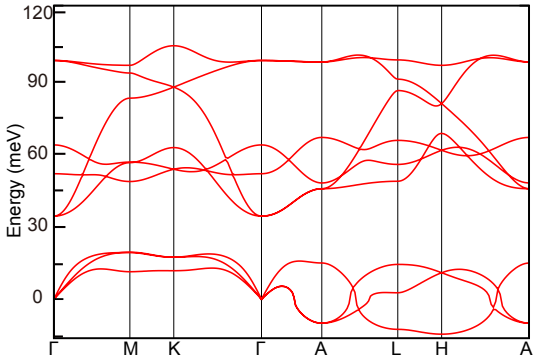

Figure S3. Calculated phonon dispersion of MoB_2 with space group No. 191.

a

q point	irreducible representations
Γ	$2E_g+3A_{1g}+3E_u+3A_{2u}$
T	$2E_g+3A_{1g}+3E_u+3A_{2u}$
L	$5A_g+3B_g+2A_u+6B_u$
F	$5A_g+3B_g+2A_u+6B_u$

Z_2 indicator class for No.166 compatibility relation is not satisfied

$Z_2\times Z_2\times Z_2\times Z_4$ indicator class for subgroup No.2 compatibility relation is satisfied

symmetry-based indicator: (1112)

Nodal lines

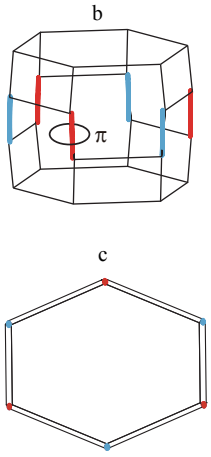

Figure S4. (a) Diagnosing procedure for topological nodal-lines near 95 meV in MoB_2. (b-c) show the side view and top view (along the [111] direction) of the nodal-lines, respectively.

CURVE FITTING

The phonon dynamic strucure factor, $S(\boldsymbol{Q},\omega)$, is related to the imaginary part of the phonon susceptibility, $\chi''(\boldsymbol{Q},\omega)$, via the thermal Bose-factor as:

$$\chi''(\boldsymbol{Q},\omega) = S(\boldsymbol{Q},\omega)(1-e^{-\omega/k_BT}). \quad (1)$$

All IXS data that we show in the main text has been converted from $S(\boldsymbol{Q},\omega)$ to $\chi''(\boldsymbol{Q},\omega)$ through Eq. 1.

Following the fitting procedure of former studies [5, 12], the data is fitted using a sum of the signals from different phonon modes and convoluted with the energy resolution function $R(\omega)$. Here $R(\omega)$ is found to be well described by a pseudo-Voight function

$$R(\omega) = (1-\alpha)\frac{A}{\sqrt{2\pi}\sigma}e^{-\frac{\omega^2}{2\sigma^2}} + \alpha\frac{A}{\pi}\frac{\gamma}{\omega^2+\gamma^2}. \quad (2)$$

We also include a constant offset I_c in our fitting routine, such that

$$\chi''(\boldsymbol{Q},\omega) = \sum_i \chi_i''(\boldsymbol{Q},\omega) * R(\omega) + I_c. \quad (3)$$

Here phonon modes are represented by the damped harmonic oscillator form [13]

$$\chi_i''(\boldsymbol{Q},\omega) = \frac{4A_i\gamma_i\omega\omega_i}{\pi\left[(\omega^2-\omega_i^2)^2+4\omega^2\gamma_i^2\right]}. \quad (4)$$

where A_i, ω_i and $2\gamma_i$ are the intensity, energy and full width at half maximum (FWHM) of phonon peak i at the measured momentum transfer, $\boldsymbol{Q}$. In all our fittings, the γ_i is found to be much smaller than the instrumental energy resolution, $\Delta E \sim 1.5$ meV, therefore all fitted peaks are essentially resolution limited.

The number of phonon peaks used in our fittings are based on the resolution-convoluted $S^{DFPT}(\mathbf{Q},\omega)$ shown in Fig. 3 of the main text.

We shall note that in principle the 95 meV nodal-lines can also be probed by IXS. However, since the 95 meV nodal-line is dominated by B-vibrations, following Eq. 3 and 4 in the main text, the IXS intensity near the 95 meV nodal-line is about 20 times weaker than that of the 30 meV nodal-lines, which is mainly composed of Mo-vibrations. In practice, measurement of the 95 meV modes requires 40 minutes per point in the energy scans at constant momentum transfer $\mathbf{Q}$, and hence cannot be accomplished with limited beamtime.

TOPOLOGICAL INVARIANTS OF THE 95 MEV NODAL-LINES

To find out the z_2 index and the topological nature of band crossings around 95 meV in MoB_2, we use the method shown in Fig. S4 (a). We first obtain the symmetry data (irreducible representations of the high symmetry points Γ, T, F and L) by DFPT theory [14–16] and find that, for the first 16 phonon modes, the symmetry data do not satisfy the compatibility relation along the $F-T$ and the $F-\Gamma$ directions. This means that band inversion exists between the 16th and 17th band along these directions. This result perfectly matches the calculated phonon dispersions shown in the main text. We then find that the compatibility relation is satisfied for subgroup No. 2, which has a nontrivial symmetry-based indicator $\mathbb{Z}_2\times\mathbb{Z}_2\times\mathbb{Z}_2\times\mathbb{Z}_4$. We therefore continue by using the indicator formula for space group No. 2 (Eq. 1 and 2 in main text) and obtained the topological invariant $z_{2,1}z_{2,2}z_{2,3}z_4 = (1112)$. In the final step, based on the (1112) indicator, we find that there will be 2 mod 4 nodal lines in the BZ along the [111] direction. Each nodal line shown in Fig. S4b carries a π Berry phase, and are robust against small perturbations that do not break $\mathcal{PT}$ symmetry. More detailed phonon calculations confirm that MoB_2 has two nodal lines. The 95 meV nodal-line paths are shown in Fig. S4(c) as red and blue curves.

It is worth to note that the 95 meV nodal-line is also helical along the [111] direction. However, its in-plane variation is significantly smaller than the 30 meV nodal-lines.

* hmiao@bnl.gov
† hlei@ruc.edu.cn
‡ hmweng@iphy.ac.cn
§ mdean@bnl.gov

[1] A Togo and I Tanaka, "First principles phonon calculations in materials science," Scr. Mater. **108**, 1–5 (2015).

[2] Luis Elcoro, Barry Bradlyn, Zhijun Wang, Maia G Vergniory, Jennifer Cano, Claudia Felser, B Andrei Bernevig, Danel Orobengoa, G Flor, and Mois I Aroyo, "Double crystallographic groups and their representations on the bilbao crystallographic server," Journal of Applied Crystallography **50**, 1457–1477 (2017).

[3] Georg Kresse and Jürgen Furthmüller, "Efficient iterative schemes for ab initio total-energy calculations using a plane-wave basis set," Physical review B **54**, 11169 (1996).

[4] QuanSheng Wu, ShengNan Zhang, Hai-Feng Song, Matthias Troyer, and Alexey A. Soluyanov, "WannierTools: An open-source software package for novel topological materials," (2017), arXiv:1703.07789.

[5] H. Miao, D. Ishikawa, R. Heid, M. Le Tacon, G. Fabbris, D. Meyers, G. D. Gu, A. Q. R. Baron, and M. P. M. Dean, "Incommensurate phonon anomaly and the nature of charge density waves in cuprates," Phys. Rev. X **8**, 011008 (2018).

[6] Alfred Q. R. Baron, "High-resolution inelastic x-ray scattering i: Context, spectrometers, samples, and superconductors," in *Synchrotron Light Sources and Free-Electron Lasers: Accelerator Physics, Instrumentation and Science Applications*, edited by Eberhard Jaeschke, Shaukat Khan, Jochen R. Schneider, and Jerome B. Hastings (Springer International Publishing, 2015) pp. 1–68, arXiv:1504.01098v5.

[7] M. P. Lopez Sancho, J. M. Lopez Sancho, J. M. L. Sancho, and J. Rubio, "Highly convergent schemes for the calculation of bulk and surface Green functions," Journal of Physics F Metal Physics **15**, 851–858 (1985).

[8] M P Lopez Sancho, J M Lopez Sancho, and J Rubio, "Quick iterative scheme for the calculation of transfer matrices: application to mo (100)," Journal of Physics F: Metal Physics **14**, 1205 (1984).

[9] Pingping Liu, Fang Peng, Shuai Yin, Fangming Liu, Qiming Wang, Xuhui Zhu, Pei Wang, Jing Liu, and Duanwei He, "Exploring the behavior of molybdenum diboride (mob2): A high pressure x-ray diffraction study," Journal of Applied Physics **115**, 163502 (2014),

https://doi.org/10.1063/1.4872459.

[10] Li-Ping Ding, Peng Shao, Fang-Hui Zhang, Cheng Lu, Lei Ding, Shu Ya Ning, and Xiao Fen Huang, "Crystal structures, stabilities, electronic properties, and hardness of MoB2: First-principles calculations," Inorganic chemistry **55**, 7033–7040 (2016).

[11] Q Xie, J Li, M Liu, L Wang, D Li, Y Li, and Q Chen, X, "Phononic weyl nodal straight lines in high-temperature superconductor mgb_2," preprint arXiv:1801.04048v1 (2018).

[12] Hu Miao, TT Zhang, Le Wang, Derek Meyers, AH Said, YL Wang, YG Shi, HM Weng, Zhong Fang, and MPM Dean, "Observation of double weyl phonons in parity-breaking fesi," Physical review letters **121**, 035302 (2018).

[13] B. Fåk and B. Dorner, "Phonon line shapes and excitation energies," Physica B: Condensed Matter **234**, 1107 – 1108 (1997).

[14] Hoi Chun Po, Ashvin Vishwanath, and Haruki Watanabe, "Symmetry-based indicators of band topology in the 230 space groups," Nature Communications **8**, 50 (2017).

[15] Zhida Song, Tiantian Zhang, Zhong Fang, and Chen Fang, "Quantitative mappings between symmetry and topology in solids," Nature communications **9**, 3530 (2018).

[16] Zhida Song, Tiantian Zhang, and Chen Fang, "Diagnosis for nonmagnetic topological semimetals in the absence of spin-orbital coupling," Physical Review X **8**, 031069 (2018).